CYCLIC VARIATIONS OF CME VELOCITY

E. V. IVANOV and V. N. OBRIDKO
Institute of Terrestrial Magnetism, Ionosphere and Radio Wave Propagation, 142190, Troitsk, Moscow Region, Russia

(Received 10 November 1999; accepted 19 September 2000)

Abstract. The semiannual mean CME velocities for the time interval of 1979–1989 have been analyzed to reveal a complex cyclic variation with a peak at the solar cycle maximum and a secondary peak at the minimum of the cycle. The growth of the mean CME width is accompanied by a growth of the mean CME velocity. It is shown that the cyclic variations of the mean CME velocity and the mean CME width are associated with the cyclic variations of the large-scale magnetic field structure and that the secondary peak of the semiannual mean CME velocity in 1985–1986 is due to a significant contribution of fast CMEs with a width of $\sim 100^\circ$ at the minimum of the cycle. This peak is supposed to be due to the increasing role of the global large-scale magnetic field system with a characteristic size of cells of $\sim 70^\circ - 100^\circ$ at the minimum of the cycle and the respective particularities of the large-scale magnetic field configuration in the corona.

1. Introduction

A coronal mass ejection (CME) is one the most powerful geoeffective events of solar activity. The number of papers that analyze the measured CME properties, including their occurrence rates, location relative to the solar disk, angular widths, and speeds, is large (Kahler, 1992; Gosling, 1993; Hundhausen, 1993; Webb, 1992, 1995, 1997). Some evidence for a CME relation to the heliospheric current sheet (HCS), and thus, to the large-scale solar magnetic fields (LSMF), is available in papers by Hundhausen (1993) and Webb *et al.* (1997). Ivanov, Obridko, and Shelting (1997) and Ivanov *et al.* (1999) compared the locations and occurrence rates of CMEs with the main LSMF characteristics and arrived at the conclusion that CME events were caused by interaction of two large-scale field systems. One of them (the global system of open magnetic fields) determines the location of CMEs and another (the system of closed magnetic fields) – their occurrence rate. The former manifests itself in the photosphere as a system of elements with a typical size of $\sim 70^\circ - 110^\circ$ and is characterized by a reduced differentiality of rotation. It is observed in the photosphere as the sectoral component of the solar magnetic field. In the corona and in interplanetary space, it is connected with the heliospheric current sheet and determines the sector structure of the interplanetary magnetic field. This system will be called henceforth the first LSMF system. Another large-scale field system appears in the photosphere as a system of closed magnetic fields with element sizes of $\sim 30^\circ - 40^\circ$ (Ivanov, 1986, 1994, 1995, 1996; Ambrož, 1992).

Solar Physics **198:** 179–196, 2001.

It seems to be due to differentially rotating magnetic fields that lie at small depths and manifest themselves as active regions or plages (Ivanov, 1986, 1994, 1995, 1996). We shall call it the second LSMF system. These two field systems and their interaction are considered in more detail in Ivanov (1994, 1995, 1996) and Obridko and Shelting (1999).

The main objective of this work is to investigate the cyclic variation of the mean CME velocity and its relation to the cyclic variation of the large-scale magnetic field structure. We shall also demonstrate that the secondary peak of the semiannual mean CME velocity at the minimum of the cycle is due to a significant contribution of fast CMEs ($V > 400$ km s^{-1}) with a width of $\sim 100^\circ$.

Section 2 describes the data, selected for the analysis. Section 3 is devoted to the study of cyclic variations of the semiannual mean CME velocity and width. Section 4 is devoted to their dependence on the structure variations of the large-scale magnetic field. In Section 5 we discuss the results.

2. Observation Data

To investigate the cyclic variation of the semiannual mean CME velocity and angular width, as well as their relation to the structure variations of the large-scale magnetic field, we have used the catalogues of CME data from the Solar Maximum Mission satellite (Burkepile *et al.*, 1993), and from P78-1 (Howard *et al.*, 1991). The coronagraph's duty cycle for all years following the 1984 SMM repair was quite high, with complete coverage averaging 78% of the available orbits each year. Annual values for the duty cycle have been published by MacQueen and St. Cyr (1991). We made no additional attempts to correct our calculations for the duty cycle of either the P78-1 or SMM coronagraphs. But we compared the CME data from SMM and P78-1 for the time intervals when observations were carried out on both satellites. This comparison revealed some systematic differences that concerned, first of all, the estimates of CME angular widths and, to a smaller extent, their apparent latitudes. As a rule, the mean CME widths estimated from SMM data are by about $10^\circ - 30^\circ$ greater than those obtained from P78-1. This systematic difference is obviously due to different instrumental facilities of the satellites and different recording procedures. In Section 3, we try to make consistent the CME widths from SMM and P78-1, proceeding from the relationship between the CME velocities and widths. As for the CME velocity distributions, they were practically the same in both databases, which allowed a general catalogue of CME velocity data to be compiled for the analysis of CME velocities. In the case when more than one velocity value was given for a CME in the Burkepile and St. Cyr Catalogue, we used only one value for the leading edge of CME. When an acceleration of a CME was observed, we took the maximum velocity. Besides, we have excluded the CME events with undefined or zero velocities, as well as several CME events

from the P78-1 data with widths $W = 360°$. All other CME events from SMM and P78-1 had angular widths $W \leq 180°$.

3. Cyclic Variations of Semiannual Mean CME Velocities and Widths

Figure 1 illustrates the CME velocity distribution based on the data from the general catalogue of CME velocities for 1979–1989. As seen from the figure, the scatter of velocities is so great that, at first sight, no dependence of CME velocity on the phase of the cycle can be inferred. As in the case of solar flares, the properties of each particular CME event obviously depend on the particular occurrence conditions. However, we believe that the mean statistical parameters of CME are determined by the typical features of the large-scale structure of solar magnetic fields, so that the CME velocities averaged over a long time interval (e.g., a year or half a year) must represent the cyclic variation of this structure. In fact, the CME velocities approximated by a 10th-order polynomial (solid line in Figure 1) reveal some cyclic variations with the maxima in 1982, 1986, and 1989. The same variations are evident in the envelope of CME velocity distributions (dashed line in Figure 1), plotted over the average values of 3 maximum CME velocities for each half-year interval. Besides the cyclic variation, this curve demonstrates quasi-biennial oscillations of the maximum CME velocity.

The semiannual mean and median CME velocities and angular widths, as well as the semiannual summary CME numbers, derived separately from the SMM and P78-1 data, are represented in Figure 2 as a function of the solar cycle. The sixth-order polynomial fits for the mean CME velocity from the SMM and P78-1 data are shown with solid lines in Figure 2(a). The lower dashed curve in Figure 2(b) illustrates the CME angular widths measured on P78-1. The upper left solid line shows the same P78-1 values, recalculated to make them fit the corresponding SMM data. (The fitting method is described below.) The tenth-order polynomial fits for the median CME velocity and width from the SMM and P78-1 data are shown with dashed lines in Figures 2(a) and 2(b) (the upper dashed lines). Figure 2(c) represents the semiannual summary CME numbers. We believe that both the mean and median CME velocities and widths are characterized by the same standard error of the mean value. Therefore, to avoid overloading Figures 2 and 3, we have only plotted the error bars for the mean velocity and width points.

Figure 3 illustrates cyclic variations of the mean and median CME velocities, widths, and numbers for the data averaging intervals of a year and six months and for different start times of the averaging interval (shifted in phase by a quarter or half a year). The tenth-order polynomial fits for the semiannual mean (Figures 3(a–c)) and median (Figures 3(d) and 3(e)) CME velocities and widths are shown with solid and dashed lines for averaging intervals starting at the beginning of each half-year interval and shifted by a quarter of a year, respectively. (Sixth-order polynomials are used for the widths from P78-1 data.) As seen from the figure,

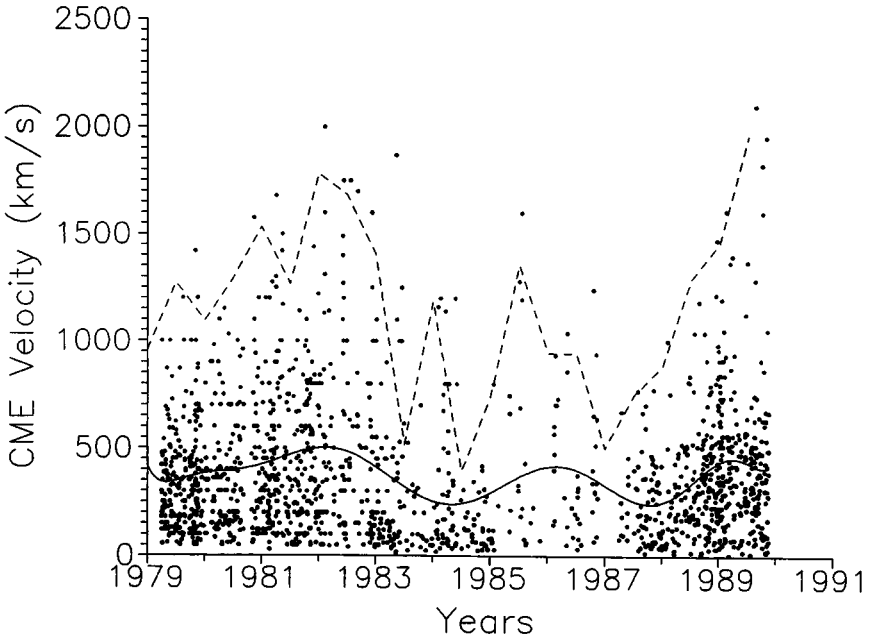

Figure 1. CME velocity distribution in 1979–1989. The *solid line* shows the CME velocities approximated by a 10th-order polynomial. The *dashed line* is the envelope of the CME velocity distribution, plotted by averaging three maximum-velocity values for each half-year interval.

the cyclic variations of CME velocity, width, and number do not depend on the choice of the data averaging interval, its start time, and the use of the mean or median values. Henceforth, we shall only deal with the mean values. But, in fact, the obtained results are valid for the median values, too.

Let us consider the relationship between the CME velocities and widths, separately for the SMM and P78-1 data. Figure 4 illustrates the CME velocity V as a function of the CME angular width W separately for (a) SMM, (b) P78-1, and (c) for both data bases. One can readily see that V grows linearly with the growth of W as $V = a + bW$. However, the a and b coefficients differ in the expressions for the SMM and the P78-1 data. Let us regard the SMM data as the main data base. Then, the $V(W)$ dependence for P78-1 must be modified to fit the similar expression for SMM. As a result, V will remain unchanged, a and b will be the same as in the expression for SMM, and W will became greater than the measured P78-1 values. In this case, the $V(W)$ approximating lines for SMM and P78-1 will coincide (Figure 4(d)).

The upper solid line in Figure 2(b) represents the new corrected values of the angular mean CME widths from P78-1. Note that, in the process of fitting, some

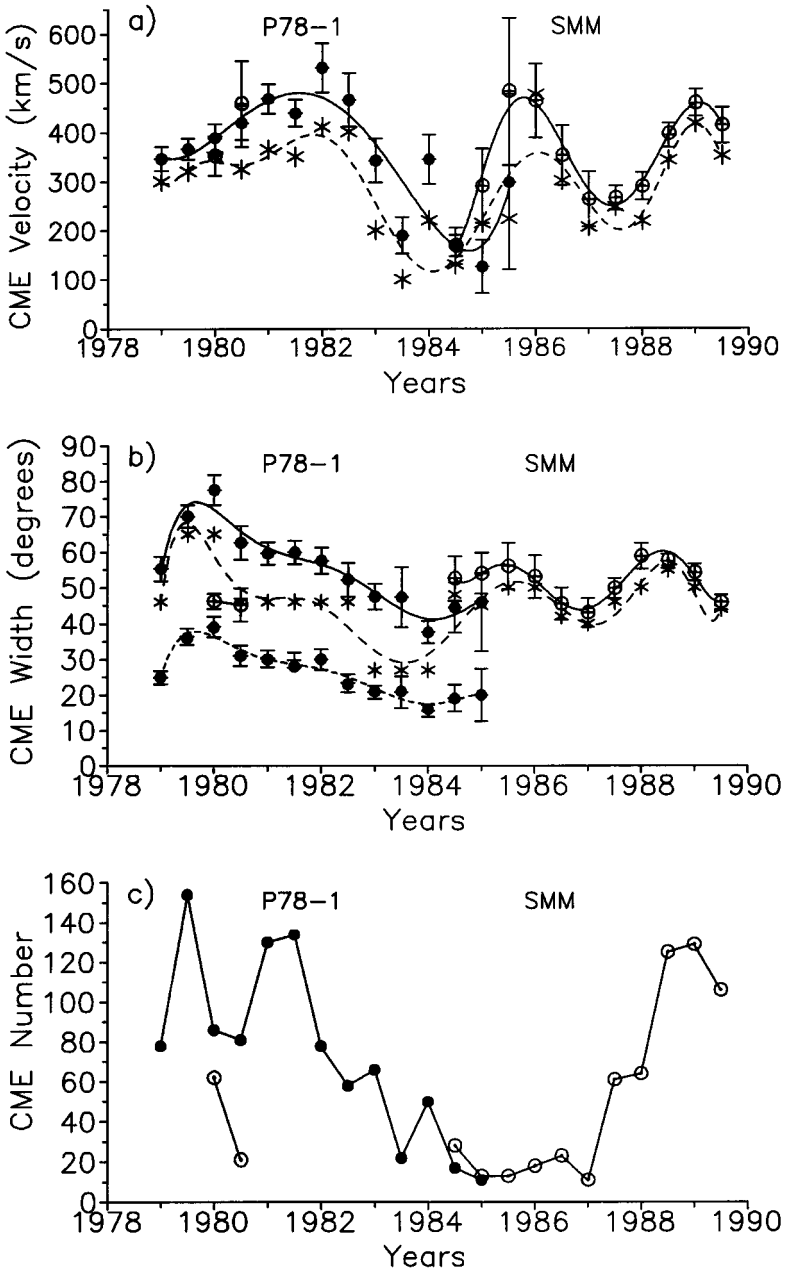

Figure 2. The semiannual mean and median (a) CME velocities, (b) angular widths, and (c) semi-annual summary CME numbers, derived separately from the SMM and P78-1 data bases. The *solid lines* in (a) and (b) show the sixth-order polynomial fits for the mean CME velocity from SMM and P78-1. The *lower dashed line* in (b) corresponds to the measured CME angular widths from P78-1, the *upper left solid line* shows the P78-1 angular widths re-calculated to fit the corresponding SMM values. The 10th-order polynomial fits for the median CME velocities and widths from the SMM and P78-1 data are shown with *dashed lines* in panels (a) and (b) (the *upper dashed line*).

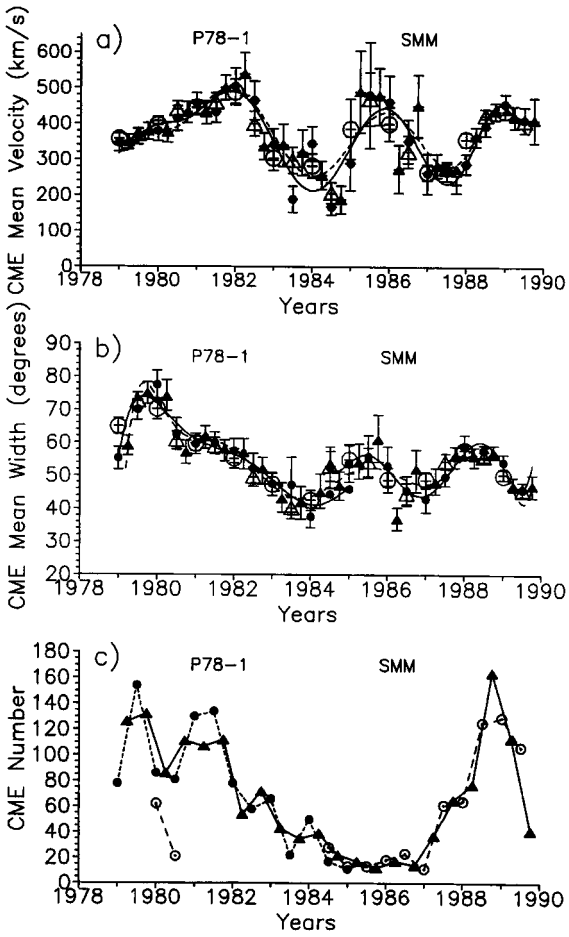

Figure 3a–c

Figure 3. Cyclic variations of (a–c) the mean and (d, e) median CME velocity, angular width, and number for different averaging intervals and different start times of the averaging interval. The *filled circles* and *triangles* in (a), (b), (d), and (e) show, respectively, the semiannual intervals starting at the beginning of each half-year interval and shifted by a quarter of a year. In the case of the mean CME velocity (a–c), the *open circles* refer to the annual intervals starting at the beginning of each year and the *open triangles*, to the annual intervals shifted by half a year. For the median CME velocity (d, e), the *open circles* (SMM data) and *squares* (P78-1 data) refer to the annual intervals starting at the beginning of each year, and the *open triangles* (SMM data) and *diamonds* (P78-1 data) to the annual intervals shifted by half a year. The *open* (SMM data) and *filled* (P78-1 data) *circles* in panel (c) denote the semiannual intervals starting at the beginning of each half-year interval, the *filled triangles* refer to the semiannual intervals shifted by a quarter of a year. The tenth-order polynomial fits (sixth-order for the width from the P78-1 data) for (a–c) the semiannual mean and (d, e) median CME velocities and widths are shown with *solid* and *dashed lines* in Figure 3. The data approximated by *dashed lines* are shifted in phase relative to the data approximated by *solid lines* by a quarter of a year.

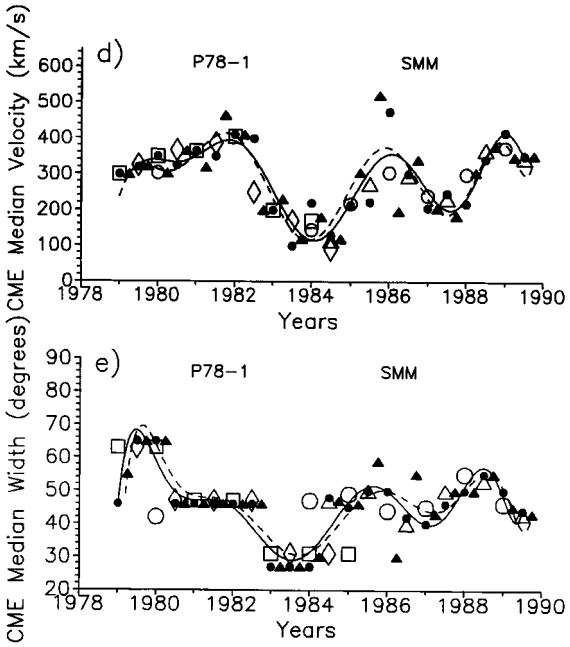

Figure 3d, e

CME angular widths from P78-1 became greater than 180° and were excluded. However, they are not numerous and do not much influence the obtained results.

As seen from Figure 2, the mean CME velocity and width (unlike the number of CME events) display a cyclic variation that does not coincide with the well-known Wolf number curve. Besides the noticeable peaks in the vicinity of the maxima of solar cycles 21 and 22 (1981–1982, 1989), the semiannual mean CME velocities and widths display a secondary peak from the second half of 1985 until the first half of 1986.

We constructed distributions of CME numbers as a function of velocity for each half-year interval with a step of 100 km s^{-1} (absolute semiannual CME distributions). Thereafter, we constructed a semiannual distribution where the number of CMEs for each velocity step was divided by the total semiannual CME number. Hereinafter, we shall call such distribution a relative velocity distribution. Similar distributions were constructed for the angular CME widths at a step of 10°. Figure 5 illustrates cyclic variations of the absolute and relative (in percent) semiannual CME distributions as a function of velocity and width for 1979–1989. The distribution of CMEs in width for 1979–1983 and the first half of 1984 was plotted using the fitted CME widths from P78-1. The measured CME widths were smoothed by moving 20° intervals to eliminate artificial 5° stratification due to rounding off the P78-1 data. The fitting to SMM data increases stratification up to ∼10°. The absolute semiannual CME distributions in velocity and width for 1979–1989

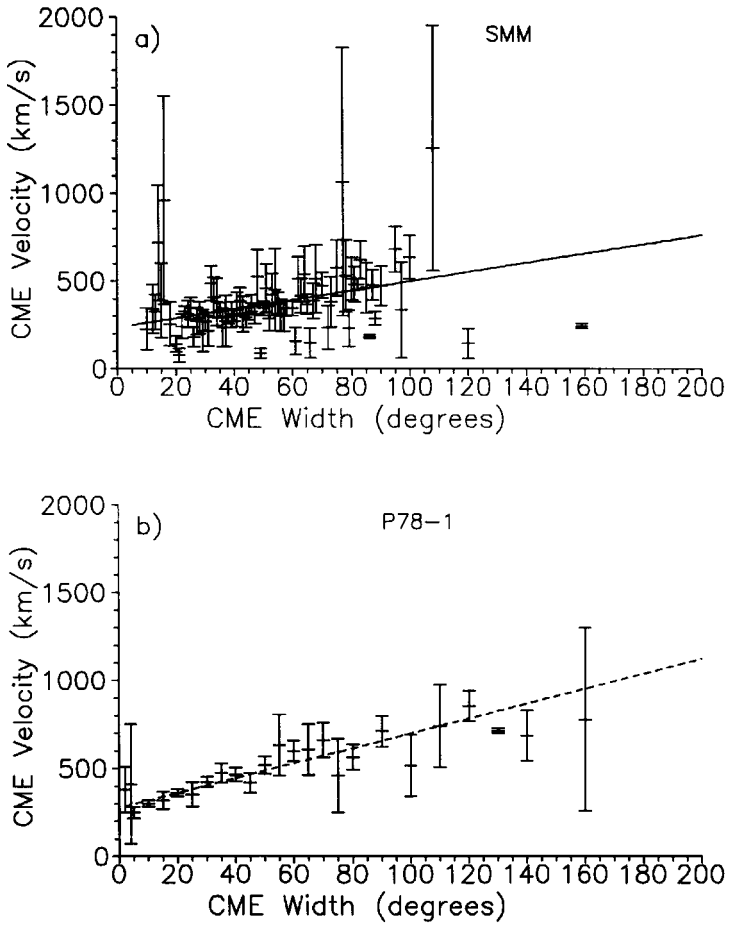

Figure 4a, b

Figure 4. The CME velocity, V, as a function of the CME angular width, W, for (a) SMM data, (b) P78-1 data, (c) SMM and real P78-1 data, (d) SMM and 'fitted' P78-1 data.

display the well-known 11-year and quasi-biennial cyclic variations. Besides, the variations of relative semiannual CME distributions in velocity and width reveal a relative increase of the number of fast ($V > 400$ km s^{-1}) and wide ($W \geq 40$–$50°$) CMEs at the minimum of the 11-year cycle. This fact seems to explain the secondary peak of the semiannual mean CME velocity in the second half of 1985 and the first half of 1986. To check this hypothesis, let us consider Figures 6–9.

Let us consider the cyclic variation in the absolute and relative annual distribution of CME widths separately for slow ($V < V_b$) and fast ($V > V_b$) CMEs. The choice of the border velocity, V_b, used to separate the slow and fast CMEs is, of course, a bit arbitrary. The choice of $V_b = 400$ km s^{-1} is based on the relative CME velocity distribution in Figure 5. However, either absolute or relative distributions

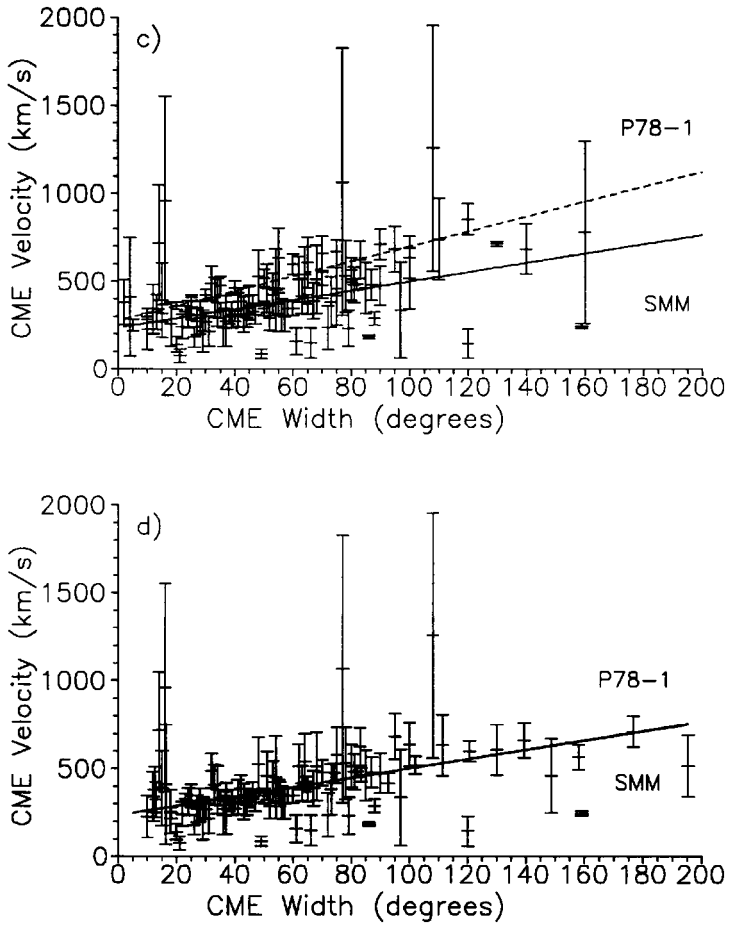

Figure 4b, c

of CME widths do not depend on the chosen V_b (at least, up to $V_b = 600$ km s^{-1}). Figures 6(a) and 6(b) illustrate the absolute and relative annual distributions of CME widths separately for slow (two panels at the top) and fast (two panels at the bottom) CMEs for the period of 1979–1989 at $V_b = 400$ km s^{-1} (Figure 6(a)) and $V_b = 600$ km s^{-1} (Figure 6(b)). Variations in the absolute and relative distribution of CME widths do not change as the start time of the annual interval shifts by half or a quarter of a year. To save space, we do not show here these distributions, which are absolutely similar to those illustrated in Figures 6(a) and 6(b). All figures clearly display an additional peak of the relative number of fast CMEs with $W \sim 100°$ at the minimum of the 11-year cycle (1985–1986). This peak is absent in the distribution of slow CMEs.

Our results for the period of 1985–1986 are based on the analysis of a relatively small number of CMEs (Figure 7(b)). Their total annual number ranges from 25 to 40 events depending on the start time of the averaging interval. However this

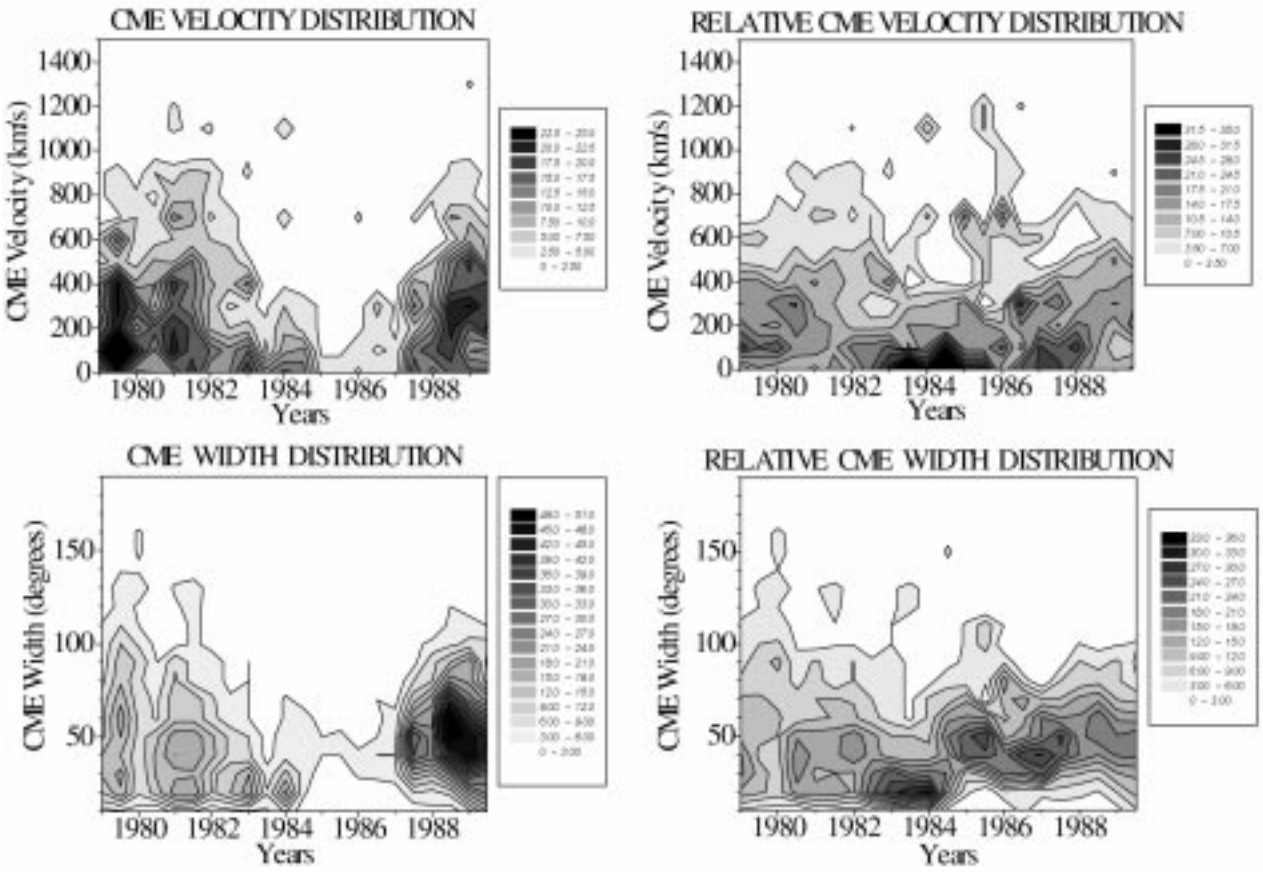

Figure 5. Variations of the absolute and relative (in %) semiannual CME distributions in velocity and width for 1979–1989.

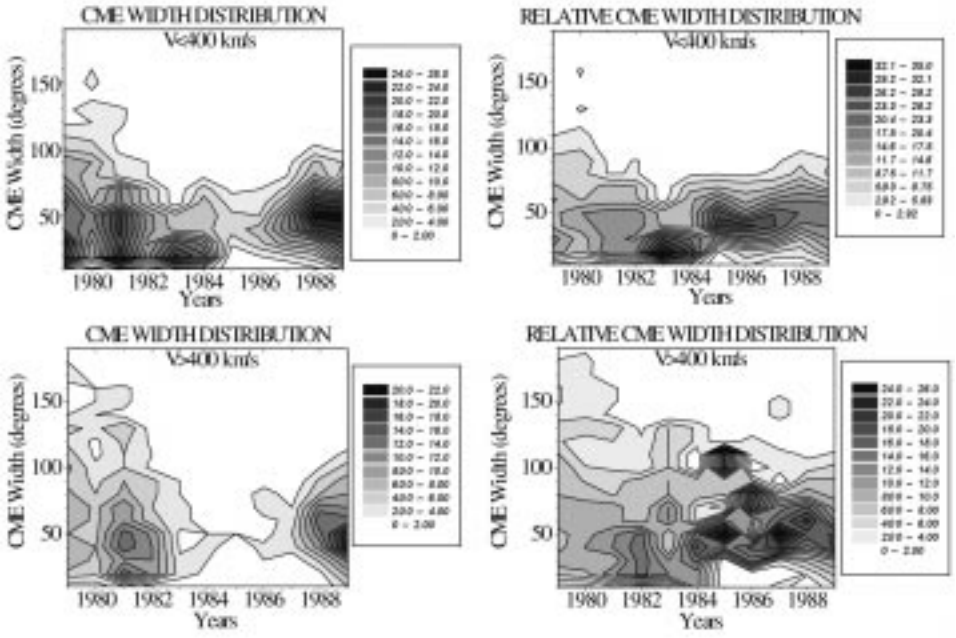

Figure 6a. Variations in the absolute and relative (in %) semiannual distribution of CME widths for slow (*top*) and fast (*bottom*) CMEs for $V_b = 400$ km s^{-1}.

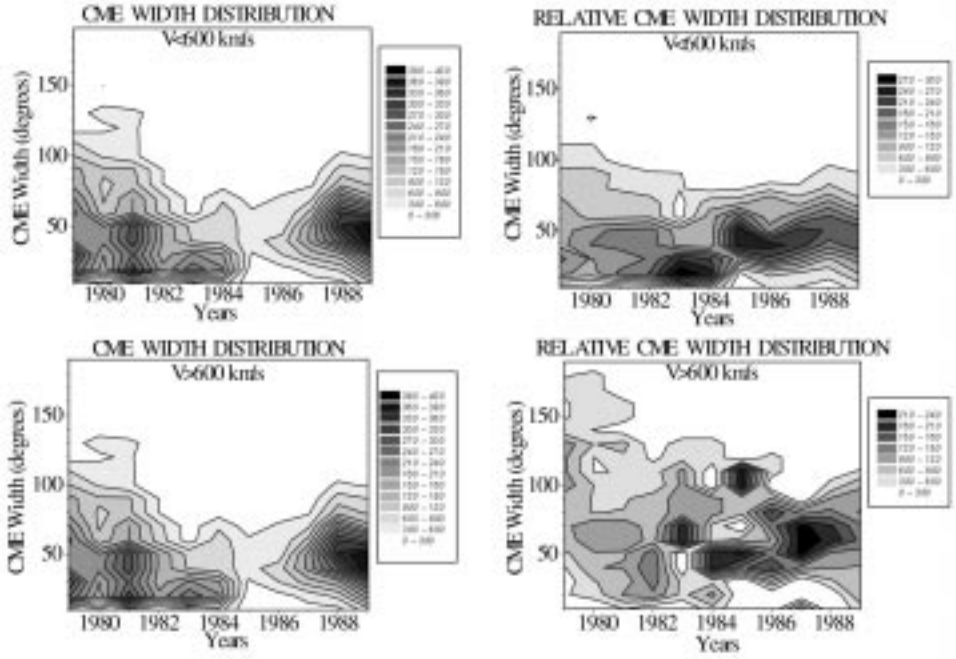

Figure 6b. Variations in the absolute and relative (in %) semiannual distribution of CME widths for slow (*top*) and fast (*bottom*) CMEs for $V_b = 600$ km s^{-1}.

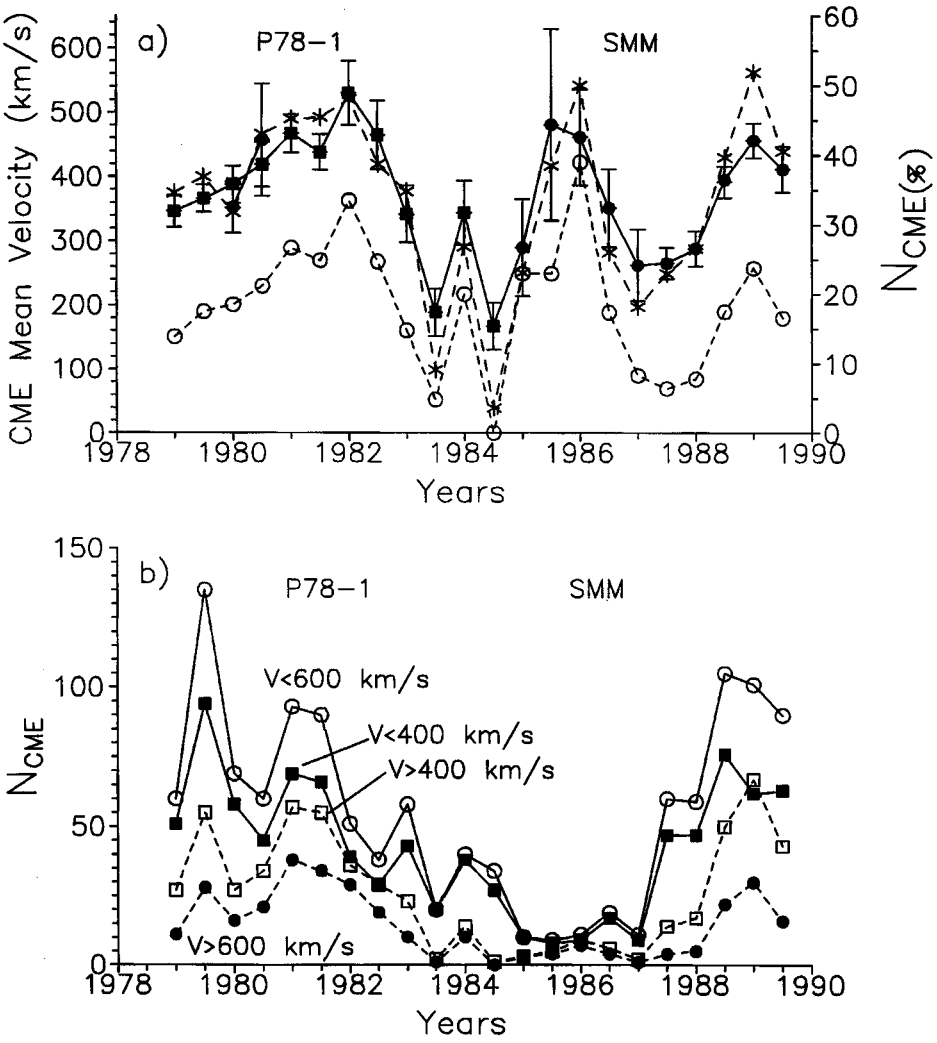

Figure 7. Cyclic variations in (a) the relative semiannual summary number of fast CMEs for $V_b = 400$ km s^{-1} (*dashed line with asterisks*) and $V_b = 600$ km s^{-1} (*dashed line with open circles*) and the semiannual mean CME velocity (*solid line*); and (b) variations in the semiannual summary number of slow and fast CMEs for $V_b = 400$ km s^{-1} and $V_b = 600$ km s^{-1}.

secondary peak of the semiannual mean CME velocity at the minimum of the 11-year cycle is not apparently related to a particular single active region. The duration of this velocity increase is no less than a year and does not depend on the chosen length or start time of the averaging interval.

Figure 7 shows (a) cyclic variations of the relative semiannual summary number of fast CMEs for $V_b = 400$ km s^{-1} and $V_b = 600$ km s^{-1} (solid lines) together with variations of the semiannual mean CME velocity (dashed line) and (b) variations

of the semiannual summary number of slow and fast CMEs for $V_b = 400$ km s^{-1} and $V_b = 600$ km s^{-1}. It should be noted that, unlike the ordinary cyclic curve for CME numbers with the extrema at the maximum and minimum of the solar cycle (Figure 7(b)), variations of the semiannual mean CME velocity display a peak at the minimum of the cycle (1985–1986) in addition to the peaks in the maximum epochs (1981–1982, 1989). One can also see that fast CMEs display an extra maximum of the relative number at the minimum of the solar cycle, comparable with the maxima of the relative semiannual summary numbers of fast CMEs at the maxima of cycles 21 and 22. The comparison of the lines in Figure 7(a) shows an amazing similarity of all three variations. This implies that the cyclic variation of the semiannual mean CME velocity is mainly determined by the relative number of the fast CMEs. Figure 7(b) shows also that, besides the cyclic variation, the CME numbers display noticeable quasi-biennial variations.

Figure 8 represents (a) cyclic variations of the semiannual sums of CME velocity squared, ΣV^2, separately for the slow and fast CMEs; (b) variation of the ratio of ΣV^2 for the fast CMEs to ΣV^2 for the slow CMEs separately for $V_b = 400$ km s^{-1} and $V_b = 600$ km s^{-1}; and (c, d) semiannual sums of the CME velocity squared, divided by the total CME number for each half-year interval ($\Sigma V^2/n$), separately for the slow (c) and fast (d) CMEs.

Assuming that the summarized semiannual CME energy is proportional to ΣV^2, we can readily see that, though the slow CMEs exceed in number the fast ones (Figure 7(b)), the latter make the principal contribution to the total CME energy. This contribution was the largest in the epochs near the maximum of the 11-year cycle (1981–1982, 1989), when the most powerful CME events were recorded. The contribution of the fast CMEs is also noticeable in 1984, as well as at the minimum of the cycle in 1986, when their relative contribution was the largest. We should also mention a noticeable quasi-biennial variation both of the number, and of the total energy of CMEs during the 11-year cycle.

The mean CME power for each half-year interval, $\Sigma V^2/n$, behaves in a different way for slow (Figure 7(c)) and fast (Figure 7(d)) events. $\Sigma V^2/n$ for slow CMEs displays a usual 11-year cycle with a small additional peak at the cycle minimum. Contrary to that, the $\Sigma V^2/n$ curve for fast CMEs considerably differs from the usual cycle curve. The largest maximum on this curve is observed at the minimum of the Wolf number cycle (1985). This peak is much higher than the peaks at the maxima of the Wolf number cycle. Quasi-biennial variations (1–2 years) are also present on this plot.

4. Relevance of the CME Velocity and Width to the Large-Scale Magnetic Field Structure

Let us consider the relationship between the cyclic variation of the CME velocity, width, and numbers and the cyclic curve of the index of the effective solar

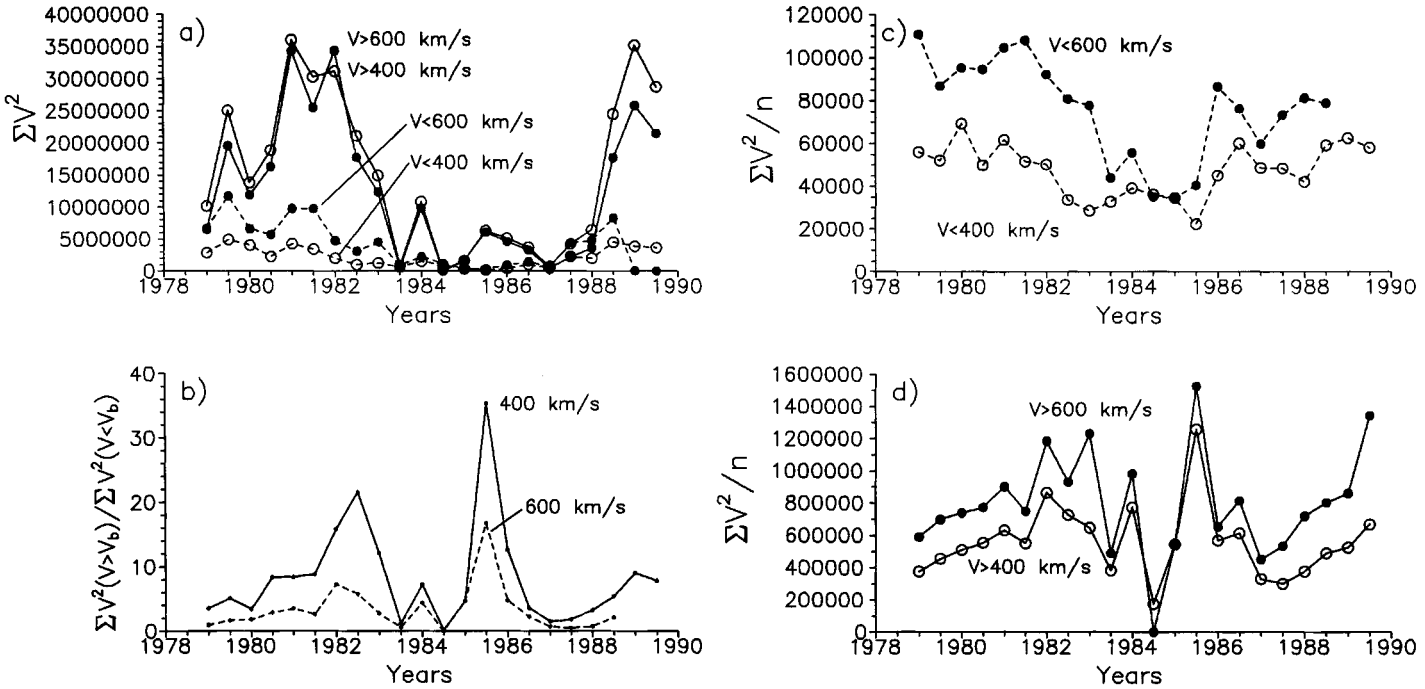

Figure 8. (a) Cyclic variations in the semiannual summary velocity squared, ΣV^2, separately for slow and fast CMEs; (b) the ratio of ΣV^2 values for the fast and slow CMEs for $V_b = 400$ km s^{-1} and $V_b = 600$ km s^{-1}; (c, d) semiannual sums of the CME velocities squared, divided by the number of CMEs for each half-year interval, $\Sigma V^2/n$, separately for (c) the slow and (d) fast CMEs.

multipole, n, that characterizes the typical scale of the large-scale magnetic field structure.

The index of the effective solar multipole,

$$n = -0.5lg(I_{ss}/I_{ph})/lg(2.5),$$

is determined by taking the logarithm of the ratio of the $I(B_r)$ value at the source surface, I_{ss}, to that in the photosphere, I_{ph}, (Ivanov, Obridko, and Shelting, 1997). The energy index of the global magnetic field, $I(B_r)$, is by definition $I(B_r) = \langle B^2 \rangle$, where $\langle B^2 \rangle$ is the square intensity of the magnetic field radial component averaged over a surface of radius r (Obridko and Ermakov, 1989; Obridko and Shelting, 1992). The indices $I(B_r)$ and n are calculated under potential approximation by using the calculation procedure where the components of the solar magnetic field are represented in the form of Legendre polynomials. The index of the effective solar multipole, n, describes the contribution of different components of the solar magnetic field at various stages of the 11-year solar cycle. In fact, when passing from the photosphere to the source surface, the magnetic flux changes in accordance with the expression $B_{ss} = B_{ph}r^{-n}$, where $n = 3$ for a dipole source, $n = 4$ for a quadrupole source, and $n > 4$ for a higher-order multipole source. When the field under consideration is a combined field from several sources with different weight, n can assume values from 3 to 4 (in the case of combined dipole and quadrupole sources) or higher (in the case of a higher-order multipole field). The relative contribution of the first (the global system of open magnetic fields, defined by dipole and quadrupole sources) and the second (the system of closed magnetic fields, defined by high-order multipole sources) LSMF systems changes depending on the phase of the solar cycle, so that n ranges from 3 to 5.

In Figure 9, the cyclic variation of the index, n, is superimposed on the corresponding cyclic curves of semiannual mean CME velocities, angular widths, and semiannual summary CME numbers, separately for the SMM and P78-1 data. A good agreement between n and the number of CME events was expected as it corroborated our earlier conclusion of a close relationship between the CME occurrence rate and the typical scale of the large-scale magnetic field structure (Ivanov, Obridko, and Shelting, 1997; Ivanov *et al.*, 1999). However the relationship between n and the CME velocity and width is more complicated. At the minimum of the cycle (1985–1986), the semiannual mean CME velocity and width increase together with a simultaneous growth of the typical scale of the large-scale magnetic field structure (decreasing n index). At the growth and decay phases of the cycle, they increase together with a simultaneous decrease of the typical scale of the large-scale magnetic field structure (increasing n index). This contradiction is probably due to the difference in cyclic variations of the large-scale magnetic field structure in the photosphere and corona. The predominant field system in the photosphere is a system of closed magnetic fields with a mean size of typical elements of $\sim 30^\circ - 40^\circ$, which determines the CME occurrence rate (cyclic variation). This is the system that most of the slow ($V < 400$ km s^{-1}) CMEs with an angular width

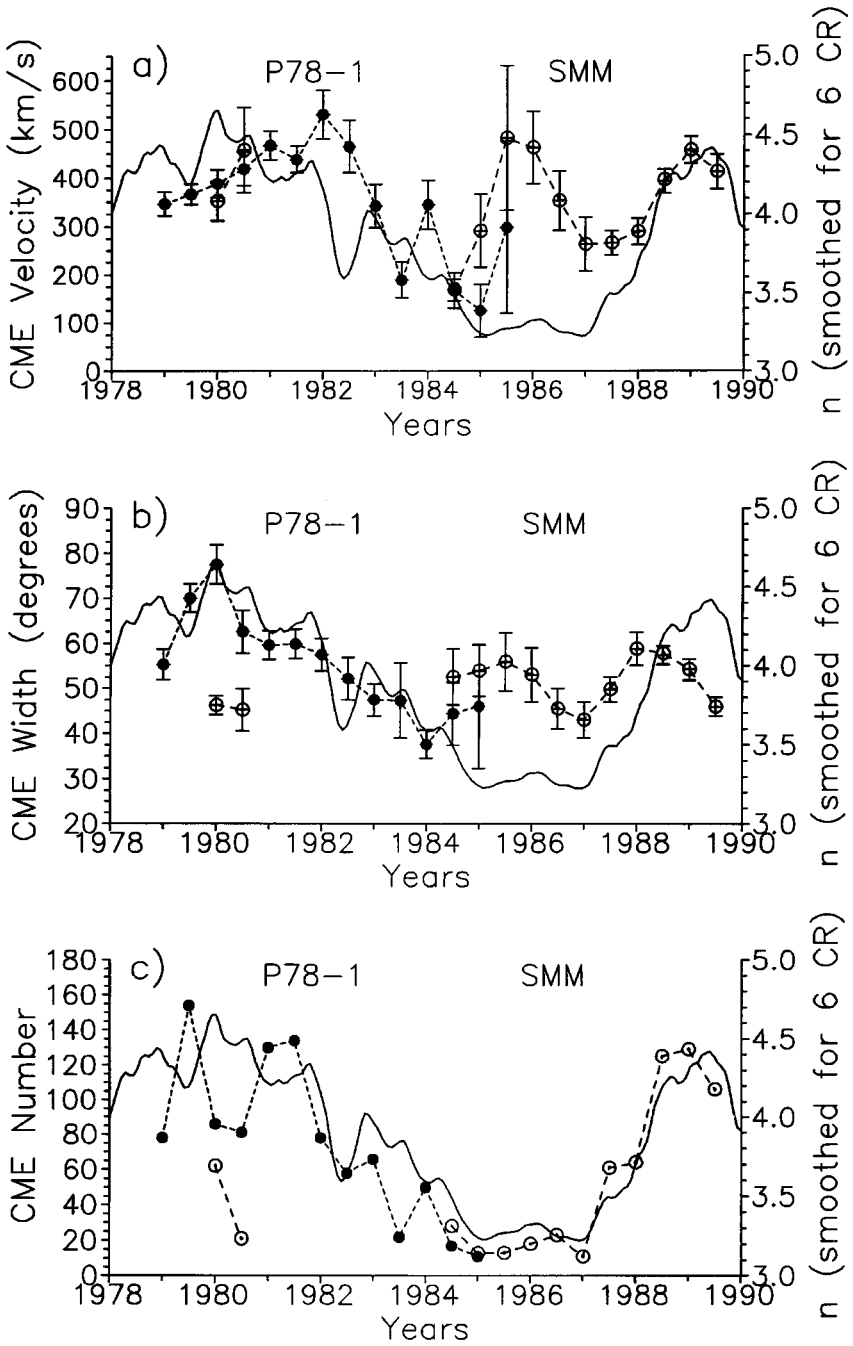

Figure 9. The semiannual mean (a) CME velocity, (b) angular width, and (c) the semiannual summary CME number (all *dashed lines*) as a function of the solar cycle with the superimposed index of the effective solar multipole, *n* (*solid line*).

$W < 40-60°$ are connected with. In the corona, the global system of open magnetic fields (OMF) prevails, with the size of typical elements of $\sim 70-110°$. This global system evidently determines the cyclic evolution of fast ($V > 400$ km s^{-1}) CMEs with an angular width $W > 60°$ ($\sim 100°$ at the minimum) and quasi-biennial variations of the CME number. Its role increases at the minimum of the Wolf number cycle. This system is likely to determine the physical characteristics of CMEs, such as their angular width and velocity.

5. Discussion of Results

The previous sections lead us to the conclusion that the cyclic behaviour of all 3 CME parameters – the velocity, the angular width, and the number – are closely related to the cyclic variation of the large-scale solar magnetic fields.

A complicated character of cyclic variations of the semiannual mean CME velocity is due to the following factors. Firstly, the relation between the CME velocity, V, and width, W, is described well enough by a linear approximation: V grows with the growth of W. While the number of CME events is mostly determined by the system of closed magnetic fields with a size of elements of $\sim 30°-40°$ prevailing in the photosphere – the second LSFM system, that is enhanced in the maximum epochs and weakens at the minimum, the CME velocity, V, and width, W, seems to be more closely related to the system of global open fields with a typical size of elements of $\sim 70°-110°$ that is predominant in the corona – the first LSMF system. Therefore the cyclic variations of the semiannual mean CME velocity and width are determined basically by the cyclic variation of the structure of large-scale magnetic fields in the corona, i.e. by the configuration of open magnetic fields. In addition, the variation of the semiannual mean CME velocity is mainly due to the variation of the relative number of fast CMEs with a velocity of $V > 400$ km s^{-1}. The relative growth of the semiannual mean CME velocity at the minimum of the 11-year cycle (the secondary peak) is due to a relative increase of the number of the wide ($W \sim 100°$) fast CMEs in that epoch. An important role in generation of the latter probably belongs to the first (global) LSMF system.

Though the slow CMEs significantly exceed in number the fast ones, the latter make a fundamental contribution to the total CME energy. This contribution is most significant in the epochs of maximum of the 11-year cycles, when the most powerful CME events tend to occur. At the same time, the relative number of the most powerful fast CMEs is the greatest at the minimum of the 11-year cycle, although the total CME number in this period is, of course, low.

We should mention a noticeable quasi-biennial variation both of the number, and of the total energy of fast CMEs during the 11-year cycle. Note that quasi-biennial variations are typical especially of the first LSFM system (the global magnetic field system that determines the 2- and 4-sector structure of the solar

magnetic field). This is additional evidence of a close relation of fast CMEs to the global system of the large-scale solar magnetic fields prevailing in the corona.

Acknowledgements

The work was supported by the Russian Foundation for Basic Research (Grants N 98-02-16189, 96-02-17054, and 07-02-1691) and the National Program for Astronomy.

References

Ambrož, P., 1992, in S. Fisher and M. Vandas, (eds.), *Proceedings of the First SOLTIP Symposium*, Vol. 21, p. 38.

Burkepile, J. T. and St. Cyr, O. C.: 1993, *A Revised and Expanded Catalogue of Mass Ejections Observed by the Solar Maximum Mission Coronograph*, High Altitude Obs., Natl. Cent. for Atmos. Res., Boulder, Colorado.

Gosling, J. T.: 1993, *J. Geophys. Res.* **98**, 937.

Howard, R. A., Sheeley, N.R., Jr., Koomen, M. J., and Michels, D. J.: 1991, *Preliminary CME List*, Washington.

Hundhausen, A. J.: 1993, *J. Geophys. Res.* **98**, 13177.

Hundhausen, A. J., Burkepile, J. T., and St. Cyr., O. C.: 1994, *J. Geophys. Res.* **99**, 6543.

Ivanov, E. V.: 1986, *Soln. Dann.* No. 7, 61.

Ivanov, E. V.: 1994, in D. N. Baker, V. O. Papitashvili, and M. J. Teague, (eds.), *Solar Terrestrial Energy Program, The Initial Results from STEP Facilities and Theory Campaigns*, Proceedings of the 1992 STEP Symposium/5th COSPAR Colloquium held in Laurel, Maryland, U.S.A., 24–28 August 1992, Pergamon, COSPAR Colloquia Series **5**, 133.

Ivanov, E. V.: 1995, *Bull. Russian Acad. Sci.* **59**, 1133.

Ivanov, E. V.: 1996, *J. Geomagn. Geoelec.* **48**, 11.

Ivanov, E. V., Obridko, V. N., and Shelting, B. D.: 1997, *Astron. Reports* **41**, 236.

Ivanov, E. V., Obridko, V. N., Nepomnyashchaya, E. V., and Kutilina, N. V.: 1999, *Solar Phys.* **184**, 369.

Kahler, S. W.: 1992, *Ann. Rev. Astron. Astrophys.* **30**, 113.

MacQueen, R. M. and St. Cyr, O. C.: 1991, *Icarus* **90**, 96.

Obridko, V. N. and Ermakov, F. A.: 1989, *Astron. Circ.* **1539**, 24.

Obridko, V. N. and Shelting, B. D.: 1992, *Solar Phys.* **137**, 167.

Obridko, V. N. and Shelting, B. D.: 1999, *Solar Phys.* **187**, 185.

Webb, D. F.: 1992, in Z. Švestka, B. Jackson, and M. Machado (eds.), *Eruptive Solar Flares*, *Lecture Notes in Physics* **399**, p. 234.

Webb, D. F.: 1995, *Rev. Geophys. Suppl.* **33**, 577.

Webb, D. F.: 1997, in E. Sagawa and M. Akioka, (eds.), *Workshop on Solar Flares and Related Disturbances*, Proceedings of a Workshop at Hitachi, Japan, January 23–25, 1996, Hiraiso Solar Terrestrial Research Center, p. 85.

Webb, D. F., Kahler, S. W., McIntosh, P. S., and Klimchuk, J. A.: 1997, *J. Geophys. Res.* **102**, 24161.